PERFORMANCE ANALYSIS OF A DUAL-FLUID CPVT SOLAR CONCENTRATOR (Water and Air)

PASERA Joanès Keneddy[1], HARITHI BEN Daoud Ben Attoumane[1], DONA Victorien Bruno[2]

[1]*PhD student, Laboratory of Applied Physics and Renewable Energies (LPADER), Ecole Doctoral Génie du Vivant et Modélisation (EDGVM), University of Mahajanga, Madagascar*
[2]*Professor, Laboratory of Applied Physics and Renewable Energies (LPADER), University of Mahajanga, Madagascar*

ABSTRACT

This study proposes an innovative approach combining a dual-fluid (water and air) photovoltaic-thermal sensor and a solar concentrator (dual-fluid CPVT), with the aim of evaluating their respective efficiencies and optimizing solar energy conversion. This cogeneration system ensures the simultaneous production of electricity and heat with enhanced efficiency, adapted to the climatic conditions of Mahajanga. A one-dimensional transient numerical model was developed and simulated using MATLAB with the Runge-Kutta method, providing an accurate assessment of the system's performance. A program was designed to evaluate the electrical and thermal performance of the hybrid dual-fluid CPVT collector, whose reliability was verified by comparison with experimental data from the literature. The integration of the solar concentrator, fins attached to the upper absorber around the parallel tubes, as well as the simultaneous use of two heat transfer fluids, significantly contributes to the improvement of heat transfer, thereby increasing the overall efficiency of the system. The results obtained highlight the strong potential of this configuration, capable of simultaneously optimizing electrical and thermal yields. This study, based on rigorous modeling and advanced simulations, makes a significant contribution to the improvement of hybrid photovoltaic-thermal systems.

Keywords : *Solar irradiation, PVT, Dual-fluid, Fins, Tubes, Cylindro-Parabolic, Performance*

1. INTRODUCTION

The optimization of solar energy conversion is a key challenge for the development of efficient and sustainable systems. Hybrid photovoltaic-thermal (PVT) collectors stand out due to their ability to simultaneously generate electricity and heat [1,2]. However, the overheating of photovoltaic cells reduces their efficiency, making the development of effective cooling solutions essential [3].

Improving the PVT system is particularly relevant for regions with high solar irradiance, such as Mahajanga (Madagascar), where elevated levels of solar radiation offer considerable potential for solar energy production. To make the best use of this resource, integrating a solar concentrator into the PVT system represents a promising technology.

Studies have demonstrated the value of various PVT-CPC system configurations using water-based heat transfer fluids aimed at improving thermal dissipation and increasing the overall efficiency of the collector. These include the works of Tripathi and Tiwari (2017), as well as Deepali Atheaya et al. (2016) on a simple absorber and tube design [4,5], those of Ahed Hameed Jaaz et al. (2010) and Mekadem and Mellouki (2022) focusing on the use of water jets [6,7], and the research by Wenzhi Cui et al. on quasi-CPC systems [8]. Other types of air-based PVT systems under concentration have also been studied. Among them are the works of Tabet Ismail (2016) on a PVT system with flat reflectors [9], as well as those of Pasera Joanès et al. (2024) on a PVT-CCPH system integrating a cylindrical-parabolic concentrator and a heliostat [10,11].

The proposed dual-fluid solar-concentrated PVT system (dual-fluid CPVT) is a fusion of water-based and air-based CPVT technologies. This hybrid system integrates both heat transfer fluids (water and air) within the same collector, thereby optimizing thermal energy recovery while maintaining an optimal temperature for the photovoltaic cells under solar concentration.

The main objective of this study is to analyze the energy performance of a hybrid dual-fluid CPVT collector in order to maximize the efficiency of solar energy conversion into electricity, as well as the simultaneous recovery of hot water and air. A compound parabolic cylindrical concentrator was used for its ability to concentrate solar radiation without the need for a complex tracking system. This allows for better radiation capture, ensures more uniform energy distribution over the PVT receiver, reduces hot spots, and thereby enhances the electrical and thermal efficiency of the system [8,12]. However, this concentration leads to an increase in the temperature of the cells, requiring efficient cooling.

To address this, an innovative cooling system has been proposed, based on the use of double aluminum alloy absorbers (one of which is equipped with fins), parallel tubes, and two heat transfer fluids circulating in the cooling channel. The extracted hot water could be used for domestic or industrial applications (heating, domestic hot water production), while the recovered hot air could be utilized for drying agricultural products, thus improving the overall energy efficiency of the system.

The work focused on the modeling and simulation of this hybrid system using MATLAB software. Mathematical models were developed for each component to obtain accurate results regarding the electrical and thermal performance of the system. The simulations will help assess cooling efficiency, the impact of the concentrator on energy production, and the optimization of design parameters to maximize the hybrid system's efficiency.

2. MÉTHODOLOGIES

2.1. Description of the system configuration under examination

The dual-fluid hybrid PVT collector consists of several distinct layers : a glass cover, photovoltaic (PV) cells, an EVA film, a Tedlar layer, an upper absorber with fins, parallel tubes, heat transfer fluids (water and air), a lower absorber, and thermal insulation. It is positioned between two symmetrical compound parabolic cylindrical collectors, receiving both direct solar radiation and the radiation reflected by these concentrators. These reflectors capture, focus, and amplify the intensity of the incident solar radiation on the surface of the dual-fluid PVT collector.

The PV solar cells generate electricity, while a portion of the solar energy is converted into heat. The water and air circulating beneath the PV module absorb this heat, thereby helping to reduce the temperature of the cells. On one side, the heated water can be stored for thermal use (heating, domestic hot water, etc.). On the other, the heated air can be evenly distributed into a drying chamber using a fan, thereby optimizing product drying through efficient airflow circulation.

The water-based PVT collector is composed of the following layers : glass, PV cells, EVA film, Tedlar, absorber, parallel tubes, heat transfer fluid (water), and thermal insulation. In contrast, the configuration of the air-based PVT collector, studied by Pasera et al. [10,11], presents differences adapted to air circulation.

Figures 1 and 2 below illustrate the configuration of a hybrid solar CPVT collector using water and CPVT using air.

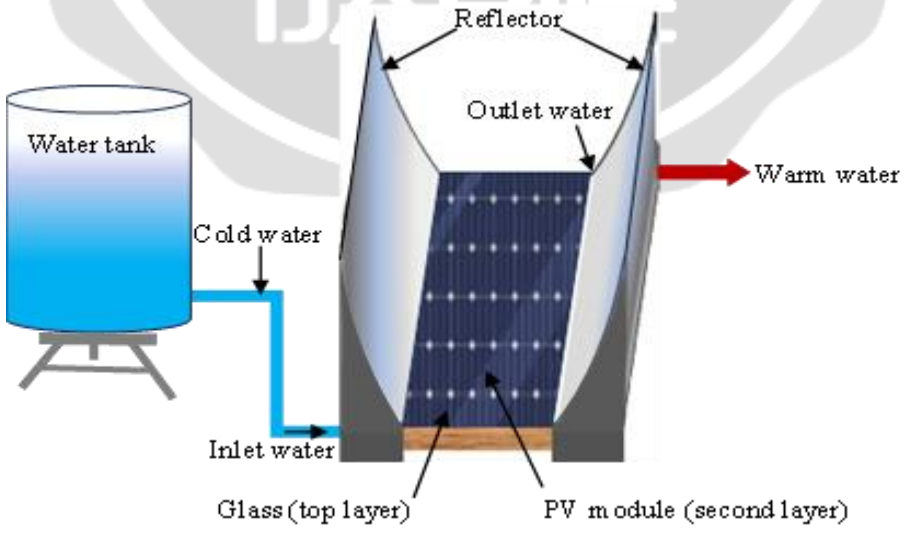

Figure 1: Schematic diagram of a water-based CPVT hybrid solar collector

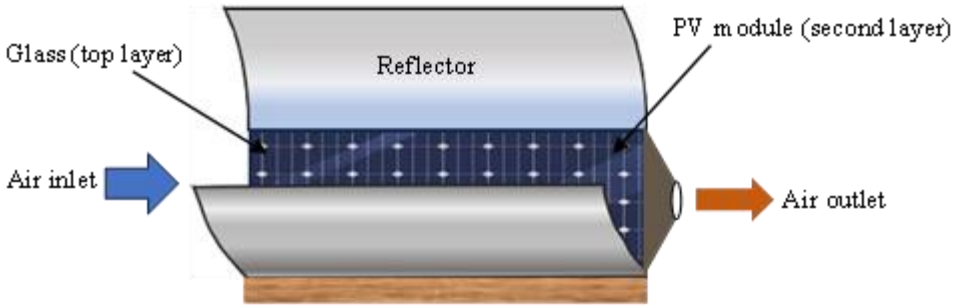

Figure 2: Schematic of an air-based hybrid CPVT solar collector

A cross-section of a dual-fluid hybrid CPVT solar collector is shown in figure 3 [9,11,13,14,15].

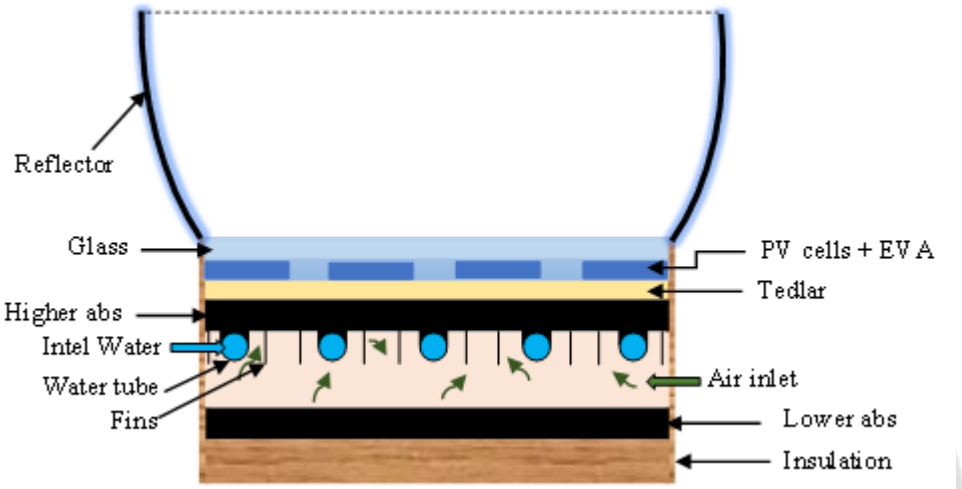

Figure 3: Front view sketch of dual-fluid CPVT system

2.2 Mathematical modeling

2.2.1 Study hypothesis

The mathematical models used to simulate the dual-fluid CPVT system are based on the following assumptions [9,10,13,14,15,16]:

- The sky can be assimilated to a black body with an equivalent temperature calculated;
- Heat transfer is considered to be one-dimensional through the layers of the system;
- The ambient temperature is the same around the sensor;
- The floor temperature is taken to be equal to the ambient temperature;
- EVA's transmission coefficient is 100%;
- The ohmic losses of the solar cells are neglected;
- The mass flow rate is uniform in the air layer duct;
- Fluid flow in the tubes is assumed to be uniform;
- The wind speed on the face of the collector is assumed to be constant;
- The thermo-physical properties of water and air vary with temperature;
- The thermal and geometric properties of the two absorbers are equal;
- The thermal properties of the fins and tubes are equal to those of the absorber;
- The effect of shading and dust on the collector is negligible;

2.2.2 Equating the system

The mathematical model of the dual-fluid CPVT system is based on the energy balance equations for the individual nodes, as shown in [7,9,10,13,14,15,16,17]:

Node 1 : outer face of glass

$$m_g Cp_g \left(\frac{dT_{g,ext}}{dt}\right) = A_g G_i C - h_{g-a}^{conv} A_g \left(T_{g,ext} - T_a\right) - h_g^{cond} A_g \left(T_{g,ext} - T_{g,int}\right) - h_{g-sky}^{rad} A_g \left(T_{g,ext} - T_{sky}\right) \quad (1)$$

Node 2 : inner face of glass pane

$$m_g Cp_g \left(\frac{dT_{g,int}}{dt}\right) = A_g \alpha_g G_i C + h_g^{cond} A_g \left(T_{g,ext} - T_{g,int}\right) - h_{g-cel}^{cond} A_g \left(T_{g,int} - T_{cel}\right) \quad (2)$$

Node 3 : PV cell

$$m_{cel} Cp_{cel} \left(\frac{dT_{cel}}{dt}\right) = A_{cel} \tau_g \alpha_{cel} G_i C + h_{g-cel}^{cond} A_{cel} \left(T_{g,int} - T_{cel}\right) - h_{cel-ted}^{cond} A_{cel} \left(T_{cel} - T_{ted}\right) - Q_{élec} \quad (3)$$

Node 4 : tedlar layer

$$m_{ted} Cp_{ted} \left(\frac{dT_{ted}}{dt}\right) = h_{cel-ted}^{cond} A_{ted} \left(T_{cel} - T_{ted}\right) - h_{ted-absh}^{cond} A_{ted} \left(T_{ted} - T_{absh}\right) \quad (4)$$

Node 5 : top absorber layer

$$\begin{aligned} m_{abs} Cp_{abs} \left(\frac{dT_{absh}}{dt}\right) = {} & h_{ted-absh}^{cond} A_{abs} \left(T_{ted} - T_{absh}\right) - h_{absh-air}^{conv} A_{absh-air} \left(T_{absh} - T_{air}\right) - U_{fin} \left(T_{absh} - T_{air}\right) \\ & - h_{absh-tube}^{cond} A_{absh-tube} \left(T_{absh} - T_{tube}\right) - h_{absh-absl}^{rad} A_{absh-absl} \left(T_{absh} - T_{absl}\right) \end{aligned} \quad (5)$$

With [11,17]: $U_{fin} = h_{absh-air}^{conv} . \eta_{fin} . A_{absh-air}$ (6)

$$\eta_{fin} = \frac{\tanh\left(L_c \cdot \sqrt{\frac{P.h_{fin}^{conv}}{\lambda_{fin} e_{fin}}}\right)}{L_c \cdot \sqrt{\frac{P.h_{fin}^{conv}}{\lambda_{fin} . e_{fin}}}} \quad A_{absh-air} = N.\left(2.H_{fin} . L_c\right) + A_{absh} + A_{tube} \quad , L_c = L + \frac{e_{fin}}{2} \text{ and } P = 2\left(L + e_{fin}\right) \quad (7)$$

Where: $A_{absh-air}$, L_c, P and e_{fin} are respectively the total available area, corrected length, perimeter and thickness of a fin.

Node 6 : tube layer

$$\begin{aligned} m_{tube} Cp_{tube} \left(\frac{dT_{tube}}{dt}\right) = {} & h_{absh-tube}^{cond} A_{absh-tube} \left(T_{absh} - T_{tube}\right) - h_{tube-wat}^{conv} A_{tube-wat} \left(T_{tube} - T_{wat}\right) \\ & - h_{tube-air}^{conv} A_{tube-air} \left(T_{tube} - T_{air}\right) - h_{tube-absl}^{ray} A_{tube-absl} \left(T_{tube} - T_{absl}\right) \end{aligned} \quad (8)$$

Node 7 : heat transfer fluid water

$$m_{wat} Cp_{wat} \left(\frac{dT_{wat}}{dt}\right) = h_{tube-wat}^{conv} A_{tube-wat} \left(T_{tube} - T_{wat}\right) - \dot{m}_{wat} Cp_{wat} \left(T_{wat,out} - T_{wat,int}\right) \quad (9)$$

Node 8: heat transfer fluid air

$$\begin{aligned} m_{air} Cp_{air} \left(\frac{dT_{air}}{dt}\right) = {} & h_{absh-air}^{conv} A_{absh-air} \left(T_{absh} - T_{air}\right) + h_{air-absl}^{conv} A_{air-absl} \left(T_{absl} - T_{air}\right) \\ & + h_{tube-air}^{conv} A_{tube-air} \left(T_{tube} - T_{air}\right) + U_{fin} \left(T_{absh} - T_{air}\right) - \dot{m}_{air} Cp_{air} \left(T_{air,out} - T_{air,int}\right) \end{aligned} \quad (10)$$

Node 9 : lower absorber layer

$$\begin{aligned} m_{absl} Cp_{absl} \left(\frac{dT_{absl}}{dt}\right) = {} & h_{air-absl}^{conv} A_{air-absl} \left(T_{air} - T_{absl}\right) + h_{absh-absl}^{rad} A_{absh-absl} \left(T_{absh} - T_{absl}\right) \\ & + h_{tube-absl}^{rad} A_{tube-absl} \left(T_{tube} - T_{absl}\right) - h_{absl-is}^{cond} A_{absl-is} \left(T_{absl} - T_{is,int}\right) \end{aligned} \quad (11)$$

Node 10 : inner face of the insulation

$$m_{is}Cp_{is}\left(\frac{dT_{is,int}}{dt}\right)=h_{absl-is}^{cond}A_{is}\left(T_{absl}-T_{is,int}\right)-h_{is}^{cond}A_{is}\left(T_{is,int}-T_{is,ext}\right) \quad (12)$$

Node 11 : outer face of the insulation

$$m_{is}Cp_{is}\left(\frac{dT_{is,ext}}{dt}\right)=h_{is}^{cond}A_{is}\left(T_{is,int}-T_{is,ext}\right)-h_{is-a}^{conv}A_{is}\left(T_{is,ext}-T_{a}\right)-h_{is-sol}^{rad}A_{is}\left(T_{is,ext}-T_{sol}\right) \quad (13)$$

2.2.3 Heat exchange coefficients

❖ **Conductive heat transfer coefficient**

In general, the conductive heat transfer coefficient between two layers of adjacent components m_i and n_i is given by the empirical relationship as follows [11,13,14] :

$$h_{m_i-n_i}^{cond}=\left(\frac{e_{m_i}}{\lambda_{m_i}}+\frac{e_{n_i}}{\lambda_{n_i}}\right)^{-1} \quad (14)$$

❖ **Coefficient of radiant heat exchange** [11,13,14].

The radiative exchange coefficient is calculated using empirical formulas as follows :

$$h_{g-sky}^{rad}=\varepsilon_g.\sigma.\left(T_{g,ext}+T_{sky}\right)\left(T_{g,ext}^2+T_{sky}^2\right) \quad (15)$$

$$h_{mi-ni}^{rad}=\sigma\frac{\left(T_{mi}+T_{ni}\right)\left(T_{mi}^2+T_{ni}^2\right)}{\left(\frac{1}{\varepsilon_{mi}}\right)+\left(\frac{1}{\varepsilon_{ni}}\right)-1} \quad (16)$$

Where: $\sigma=5,67\times10^{-8}$, Stephan Boltzmann's constant ;

$T_{sky}=0,0552.\left(T_a\right)^{1,5}$, the sky temperature is given by the Swinbank relation (17)

With : $T_a=\left[\frac{T_{a\,max}-T_{a\,min}}{2}\right].\cos\left[\frac{(TSV-12).\pi}{12}\right]+\left[\frac{T_{a\,max}+T_{a\,min}}{2}\right]$, ambient temperature (18)

❖ **Convective heat transfer coefficients** [11,13,14,15].

The Mac Adams correlation was used to determine the heat exchange between the glass and the environment :

$$h_{v-a}^{conv}=5,6+3,8V_{vent} \text{ where } V_{vent} \text{ is the wind speed} \quad (19)$$

Convective heat exchange coefficients are calculated by empirical correlations using the Nusselt number:

$$h_{air}^{conv}=\frac{Nu_{air}\lambda_{air}}{D_h} \text{ and } h_{wat}^{conv}=\frac{Nu_{wat}\lambda_{wat}}{D_{int}} \quad (20)$$

Heat transfer between absorber and fluid :

$$h_{abs-air}^{conv}=\left(\frac{e_{abs}}{\lambda_{abs}}+\frac{1}{h_{air}^{conv}}\right)^{-1} \quad (21)$$

The physical properties of air are assumed to vary linearly with temperature, in accordance with the specific expressions established by Ebrahim and Alfege [11,14] :

- Specific gravity : $\rho_{air}=1.1774-0.000359\times T_{air}$; (22)
- Specific heat : $Cp_{air}=\left[1.0057+0.000066\times T_{air}\right]\times1009$; (23)
- Thermal conductivity : $\lambda_{air}=0.02624+0.0000758\times T_{air}$; (24)
- Dynamic viscosity : $\mu_{air}=\left[1.983+0.00184\times T_{air}\right]\times10^{-5}$. (25)

In our case, the Nusselt number is calculated according to the flow regime, which is expressed by the following equations [11,18] :

- For laminar flow $\left(\mathrm{Re}_{air} < 2300\right)$

$$\mathrm{Nu}_{air} = \mathrm{N}_{\infty} + \frac{0.0019 \times \left[\mathrm{Pr}_{air} \cdot \mathrm{Re}_{air} \cdot \mathrm{D}_h / \mathrm{L}\right]^{1.71}}{1 + 0.00563 \times \left[\mathrm{Pr}_{air} \cdot \mathrm{Re}_{air} \cdot \mathrm{D}_h / \mathrm{L}\right]^{1.17}} \quad \text{(Heaton's empirical correlation)} \tag{26}$$

With : $\mathrm{N}_{\infty} = 5.4,\ \mathrm{Pr}_{air} = 0.7$

- For transient flow $\left(2300 \le \mathrm{Re}_{air} \le 6000\right)$

$$\mathrm{Nu}_{air} = 0.0214 \times \left(\mathrm{Re}_{air}{}^{0.8} - 100\right) \times \mathrm{Pr}_{air}{}^{0.4} \times \left[1 + \left(\mathrm{D}_h / \mathrm{L}\right)^{0.66}\right] \tag{27}$$

With conditions : $0.5 \le \mathrm{Pr}_{air} \le 1.5\ 2300 < \mathrm{Re}_{air} < 10^6$ and $0 < \mathrm{D}_h / \mathrm{L} < 1$

- For turbulent flow $\left(\mathrm{Re}_{air} > 6000\right)$

$$\mathrm{Nu}_{air} = 0.023 \times \left(\mathrm{Re}_{air}\right)^{0.8} \times \left(\mathrm{Pr}_{air}\right)^{0.4} \text{ (Tan and Charters' (1970) empirical correlation).} \tag{28}$$

With : $0.6 \le \mathrm{Pr}_{air} \le 160$, $\mathrm{Re}_{air} \ge 10000$ and $\mathrm{L}/\mathrm{D}_h \ge 10$

The Prandtl and Reynolds number is defined by the following relationship [10,14] :

$$\mathrm{Pr}_{air} = \frac{\mu_{air}.\mathrm{Cp}_{air}}{\nu_{air}} \text{ and } \mathrm{Re}_{air} = \frac{\mathrm{V}_{air}\mathrm{D}_h}{\nu_{air}} \text{ , with } \mathrm{D}_h = \frac{4\left(l \times \mathrm{H}_c - \mathrm{N}_{tube}\mathrm{p}\left(\mathrm{D}_{ext}/2\right)^2\right)}{2\left(l + \mathrm{H}_c\right)} \tag{29}$$

Where: D_h, ℓ, and H_c are hydraulic pipe diameter, sensor width and air pipe height respectively.

The thermo-physical characteristics of water are assumed to vary linearly with temperature [7,18,19,20,21] :

– Volume density in $\mathrm{kg.m^{-3}}$:

$$\rho_{wat} = -510.3061 + 15.19367\left(\mathrm{T}_{wat}\right) - 5.490006 \times 10^{-2}\left(\mathrm{T}_{wat}\right)^2 + 8.538520 \times 10^{-5}\left(\mathrm{T}_{wat}\right)^3 - 5.122868 \times 10^{-8}\left(\mathrm{T}_{wat}\right)^4 \tag{30}$$

– Specific heat in $\mathrm{J.kg^{-1}.K^{-1}}$:

Regime 1 : $0^{\circ}\mathrm{C} < \mathrm{T}_{wat} < 137^{\circ}\mathrm{C}$

$$\mathrm{Cp}_{wat} = \begin{bmatrix} 2.13974 - 9.68137 \times 10^{-3}\left(\mathrm{T}_{wat}\right) + 2.68536 \times 10^{-5}\left(\mathrm{T}_{wat}\right)^2 \\ -2.42139 \times 10^{-8}\left(\mathrm{T}_{wat}\right)^3 \end{bmatrix} \times 1000 \times 4.1868 \tag{31}$$

Regime 2: other temperatures

$$\mathrm{Cp}_{wat} = \begin{bmatrix} -11.1558 + 7.96443 \times 10^{-2}\left(\mathrm{T}_{wat}\right) - 1.74799 \times 10^{-4}\left(\mathrm{T}_{wat}\right)^2 \\ +1.29156 \times 10^{-7}\left(\mathrm{T}_{wat}\right)^3 \end{bmatrix} \times 1000 \times 4.1868 \tag{32}$$

– Thermal conductivity in $\mathrm{W.m^{-1}.K^{-1}}$:

$$\lambda_{wat} = -2.893282 + 3.003312 \times 10^{-2}\left(\mathrm{T}_{wat}\right) - 9.604677 \times 10^{-5}\left(\mathrm{T}_{wat}\right)^2 + 1.403673 \times 10^{-7}\left(\mathrm{T}_{wat}\right)^3 - 8.019830 \times 10^{-11}\left(\mathrm{T}_{wat}\right)^4 \tag{33}$$

– Dynamic viscosity in Pa.s :

$$\mu_{wat} = 2.340194 \times 10^{-5} \times 10^{\left(\frac{250.4833}{\mathrm{T}_{wat} - 140.0812}\right)} \tag{34}$$

Nusselt number according to flow regime [7,18,19,20,21,22] :

- For laminar flow $\left(\mathrm{Re}_{wat} < 2300\right)$

$$\mathrm{Nu}_{wat} = 4.36 \text{ with } \mathrm{L}/\mathrm{D}_{int} \geq 50 \tag{35}$$

- For transient flow $\left(2300 \le \mathrm{Re}_{wat} \le 6000\right)$

$$f_d = \left(0.79 \times \ln\left(\mathrm{Re}_{wat}\right) - 1.64\right)^{-2} \text{ where } f_d \text{is the Darcy-Weisbach friction factor.} \quad (37)$$

$$\mathrm{Nu}_{wat} = \frac{\left(f_d/8\right) \times \left(\mathrm{Re}_{wat} - 1000\right) \times \mathrm{Pr}_{wat}}{1 + 12.7\sqrt{f_d/8}\left(\mathrm{Pr}_{wat}^{2/3} - 1\right)} \text{ (Gnielinski relation).} \quad (38)$$

- For turbulent flow $\left(\mathrm{Re}_{wat} > 6000\right)$

$$\mathrm{Nu}_{wat} = 0.023 \times \left(\mathrm{Re}_{wat}\right)^{0.8} \times \left(\mathrm{Pr}_{wat}\right)^{0.4} \text{ (Dittus-Boelter relationship)} \quad (39)$$

2.3 Compound Parabolic Cylindrical Solar Concentrator [3,7,22]

The compound parabolic trough concentrator is an evolution of the simple parabolic trough concentrator, offering better solar radiation capture, a more homogeneous distribution of energy on the dual-fluid PVT receiver, thus reducing hot spots and improving the thermal and optical efficiency of the system.

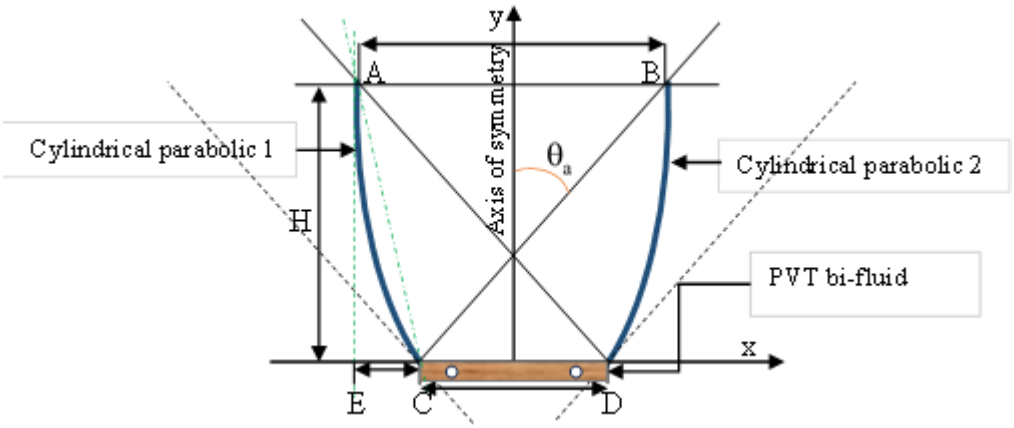

Figure 4: Compound Parabolic Cylindrical Concentrator

❖ **Geometrical considerations**

The concentrator's geometric parameters are defined in terms of aperture width, acceptance angle (θ_a) and height. The following relationships are used to determine the key dimensions [7,22,23] :

$$\begin{cases} f = \dfrac{CD\left(1 + \sin\theta_a\right)}{2}; & AB = \dfrac{CD}{\sin\left(\theta_a\right)} \\ H = \dfrac{AB + CD}{2.\tan\left(\theta_a\right)}; & C_g = \dfrac{AB}{CD} = \dfrac{1}{\sin\left(\theta_a\right)} \end{cases} \quad (40)$$

Where : f , AB , CD , H , and C_g are respectively the focal line, entrance pupil width, exit pupil width, height and geometric concentration factor of the reflector.

❖ **Energy concentration (C_e)**

The energy concentration of a solar collector is defined as the ratio between the solar energy captured by the concentrator aperture and the energy actually received by the bi-fluid PVT receiver. It depends on the optical efficiency and the geometric concentration factor [11,22].

$$C_e = C_g \times \eta_{opt} = C_g \times \left(\rho_{ccp}\right)^{N_r} \times \eta_{int} \text{ , with } \eta_{int} = 1 - e^{-C_g} \quad (41)$$

Where: ρ_{ccp} , N_r and η_{int} represent the reflectivity of the mirrors, the average number of reflections a ray undergoes before reaching the bi-fluid PVT and the interception factor.

2.4 Electrical model of a dual-fluid PVT system

The electrical behavior of the PVT system is strongly influenced by the intensity of solar irradiation and the temperature of the photovoltaic cells. For a single-diode model, the expression for the electric current leaving the photovoltaic collector is written as follows [10,15] :

$$I_{PV} = N_p.I_{ph} - N_p.I_0\left[\exp\left(q\frac{V_{PV} + I_{PV}.R_S}{n.N_S.K.T}\right) - 1\right] - \frac{V_{PV} + I_{PV}.R_S}{R_{sh}} \quad (42)$$

Where: I_{ph}, I_0, R_s, R_{sh}, q, N_s, N_p, n and K are respectively photon current, diode saturation current, series resistance, parallel resistance, electron charge, number of cells in series, number of cells in parallel, ideality factor, Boltzmann constant.

Current and voltage values vary with solar irradiation intensity and cell temperature, as shown in the following equations [10,15] :

- Output current variation: $I\left(G_iC, T_{cel}\right) = I_{ref} + \Delta I = I_{ref} + k_i\left(\frac{G_iC}{G_{ref}}\right)\Delta T + \left(\frac{G_iC}{G_{ref}} - 1\right)I_{sc,ref}$ (43)
- Output voltage variation: $V\left(G_iC, T_{cel}\right) = V_{ref} + \Delta V = V_{ref} + k_v \cdot \Delta T - R_S \cdot \Delta I$ (44)
- Short-circuit current variation: $I_{sc}\left(G_iC, T_{cel}\right) = \left(\frac{G_iC}{G_{ref}}\right) \times \left(k_i \cdot \Delta T + I_{sc,ref}\right)$ (45)
- Short-circuit current variation: $V_{oc}\left(G_iC, T_{cel}\right) = V_{oc,ref} + k_v \cdot \Delta T + n \cdot \ln\left(\frac{G_iC}{G_{ref}}\right)$ (46)

With: $\Delta T = T_{cel} - T_{ref}$ (47)

Where $k_i$and $k_v$are respectively the coefficient of variation of current and voltage as a function of temperature.

2.5 Performance of the PVT dual-fluid hybrid collector

The electrical power and thermal power produced by the PVT dual-fluid hybrid solar collector are given by the following equations [11,13,15,24] :

$$Q_{élec} = \tau_g.G_i.C.S_{cell}.\eta_{ref}.\exp\left[\beta\left(T_{cel} - T_{ref}\right)\right], \text{ where } G_i \text{ is the global solar irradiance.} \quad (48)$$

$$Q_{the,wat} = \dot{m}.Cp_{wat}.\left(T_{wat,out} - T_{wat,int}\right) \text{ and } Q_{the,air} = \dot{m}.Cp_{air}.\left(T_{air,out} - T_{air,int}\right) \quad (49)$$

$$Q_{the,PVT\_bi-fluid} = Q_{the,wat} + Q_{the,air} \quad (50)$$

The electrical and thermal efficiencies of the PVT dual-fluid hybrid solar collector are determined by the following two expressions [15,24,25] :

$$\eta_{elc} = \frac{Q_{elec}}{S_{cel} \cdot G_i \cdot C} \text{ and } \eta_{the,PVT\_bi-fluid} = \frac{Q_{the,PVT\_bi-fluid}}{S_{cel} \cdot G_i \cdot C} \quad (51)$$

The overall efficiency of a dual-fluid PVT is the sum of the thermal efficiency and the thermal efficiency equivalent to the electrical efficiency [25,26,27,28].

$$\eta_{PVT\_bi-fluid} = \eta_{the} + \eta_{elec,the} \quad (52)$$

With : $\eta_{elec,the} = \frac{\eta_{elec}}{C_f}$, where C_f is the thermal energy conversion factor between 0.2 and 0.4 [28,29].

3. RÉSULTATS ET DISCUSSIONS

3.1 Study site

The study concerns Mahajanga (15°43' S, 46°19' E), northwest of Madagascar, with 14 years of meteorological data from ASECNA. Solar irradiance was estimated using Page's model [2,11].

3.2 Electrical characteristics

The polycrystalline silicon photovoltaic collector described in Table 1 has been evaluated to international standards at 1000 $W.m^{-2}$, AM 1.5 and 25°C.

Table 1: Electrical characteristics of a KC200GT photovoltaic module [10,30]**.**

Experimental peak power P_{max}	200 W
Voltage at point of maximum power V_{pm}	26.3 V
Current at point of maximum power I_{pm}	7.61 A
Open circuit voltage V_{oc}	32.9 V
Short-circuit current I_{sc}	8.21 A
Voltage temperature coefficient k_v	–0.123 V/°C
Current temperature coefficient k_i	0.00318 A/°C
Operating temperature	–40 °C to +85 °C
Number of cells in series N_s	54
Number of parallel cells N_p	1
Reference yield	15 %
Dimension $(L \times l \times h)$	1425 mm × 990 mm × 36 mm

3.3 Component characteristics of the PVT dual-fluid hybrid module

Table 2 shows the characteristics of the various sensor components.

Table 2: Characteristics of the PVT dual-fluid hybrid collector components [14,15,24].

Components / Features	Glass	PV cell	Tedlar	Absorber	Tube	Insulation	Unit
Density	2200	2330	1300	2700	2700	60	($kg.m^{-3}$)
Specific heat	670	836	1400	900	900	700	($J.kg^{-1}K^{-1}$)
Thermal conductivity	0.93	148	0.033	237	237	0.04	($W.K^{-1}.m^{-1}$)
Emissivity	0.88	0.93	0.88	0.04	0.04	0.85	---
Thickness	0.003	0.0003	0.0005	0.005	0.001	0.004	(m)
Absorption coefficient	0.066	0.85	0.5	0.75	0.75	0.066	---
Pipe outside diameter					0.014		(m)
Inside pipe diameter					0.012		(m)

3.4 Variation in solar irradiation and ambient temperature at Mahajanga

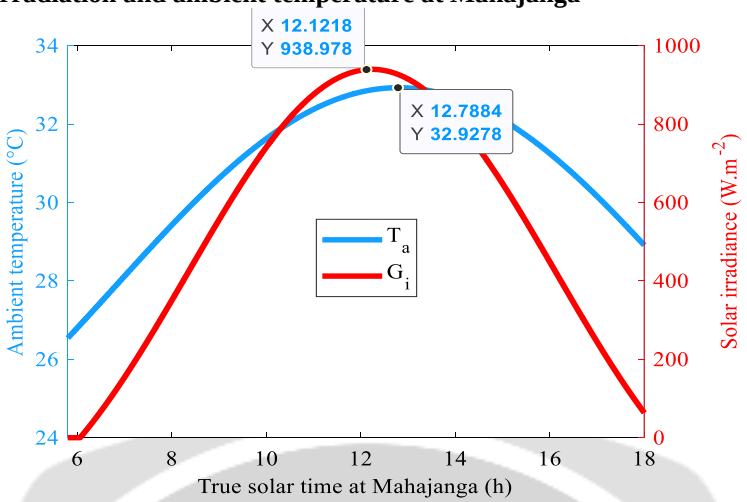

Figure 5: Temporal variation in solar irradiance and ambient temperature

Figure 5 illustrates the evolution of monthly mean hourly solar irradiance and ambient temperature as a function of the typical day of the month in question, over a 14-year period. Irradiance increases in the morning, peaks at 940 W.m^{-2} around midday, and then gradually decreases. The ambient temperature reaches a maximum of 32.92°C at 12:48 p.m., slightly after the irradiation peak, due to the thermal inertia of the materials. It is lower in the morning than in the evening.

3.5 Variation of geometric parameters and concentration ratios of the reflector

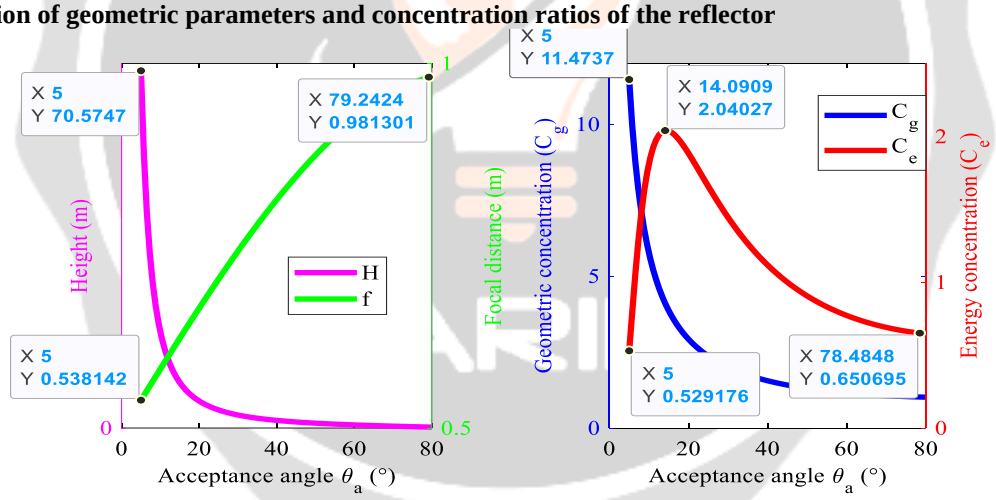

Figure 6: Variation of the reflector's geometric parameters and concentration ratios

Figure 6 shows the impact of the acceptance angle (θ_a) on the characteristics of a compound parabolic cylindrical concentrator. The height (H) decreases sharply with (θ_a), while the focal length (f) increases. A small angle requires a deeper concentrator to capture the maximum amount of radiation, whereas a larger angle reduces its height. The geometric concentration ratio (Cg) reaches a maximum of 11 before gradually decreasing, while the energy concentration ratio (Ce) peaks at 2 for an acceptance angle of 14°, then declines. This decrease is explained by increased light dispersion and optical and thermal losses, which reduce the concentration efficiency at higher angles.

3.6 Cell temperature of the different hybrid PVT collectors

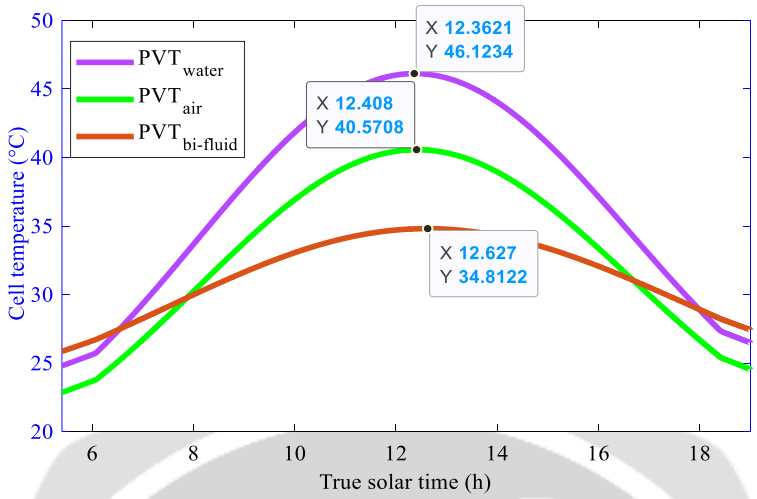

Figure 7: Cell temperature evolution for different hybrid PVT systems

Figure 7 illustrates the daily evolution of cell temperatures for three PVT collector configurations (water-based, air-based, and dual-fluid) under the climatic conditions of Mahajanga. The PV modules used are identical but integrated into different cooling systems. The mass flow rates are set at 0.02 kg·s^{-1} for water (total flow rate) and 0.028 kg·s^{-1} for air. All the curves show a gradual rise in temperature until solar noon, followed by a decrease at the end of the day. The water-based PVT exhibits the highest temperature (46 °C), due to limited heat exchange despite the high heat capacity of water. The air-based PVT reaches a maximum temperature of 40.6 °C, thanks to the integration of fins that enhance heat transfer with the air. The dual-fluid system, combining water and air, maintains the lowest temperature (34.8 °C) due to the complementary action of the two fluids and the presence of fins. Water efficiently extracts heat from the inner layers, while air facilitates thermal exchange, and the fins increase the heat transfer surface, thereby optimizing overall cooling. Thus, the dual-fluid system offers the best thermal management, limiting overheating and enhancing the energy performance of the collector. Our work is partially based on the studies of Oussama El Manssouri et al. [15,24] and Hasila Jarimi et al. [28], which also focus on dual-fluid PVT systems. However, our configuration presents specific features, particularly in terms of the cooling circuit.

3.7 Evolution of electrical characteristics (I-V and P) of hybrid photovoltaic-thermal (PVT) collectors

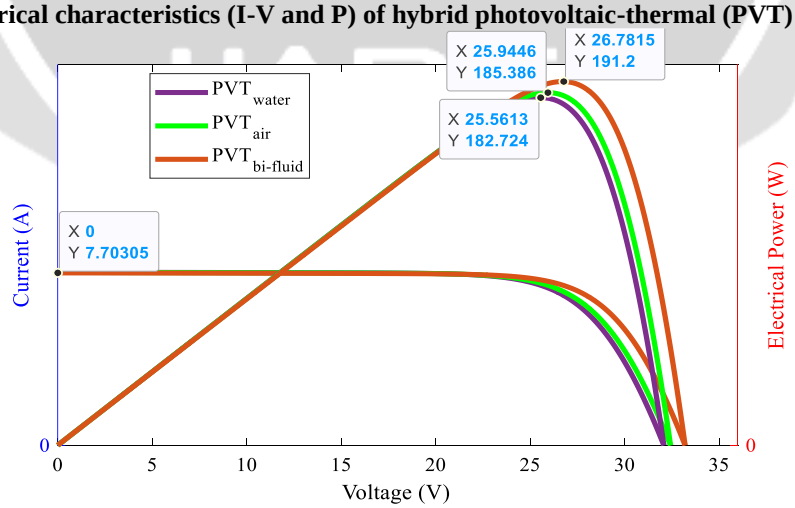

Figure 8: Current-voltage-power (I-V-P) for a PVT system using air, water and a bi-fluid

Figure 8 illustrates the comparison of the I-V-P characteristics of the water-based PVT, air-based PVT, and dual-fluid PVT solar collectors, with a water mass flow rate of 0.004 kg·s^{-1} (flowing through each tube) and an air flow rate of 0.028 kg·s^{-1}, under the same solar irradiation peak in Mahajanga. The I-V-P curves show that the dual-fluid PVT system reaches the highest electrical power output (191.2 W), followed by the air-based PVT (185.4 W), and then the

water-based PVT (182.7 W), although all exhibit a similar short-circuit current (7.7 A), confirming equal exposure to solar irradiation. These performance differences are explained by the cooling efficiency of each system, which directly affects the temperature of the photovoltaic cells. Indeed, a lower temperature improves the voltage at the maximum power point (MPP), thereby increasing the electrical power output. Thus, the electrical performance is closely linked to the thermal dissipation capacity of the PVT system.

3.8 Cell temperature of dual-fluid hybrid PVT and CPVT collectors

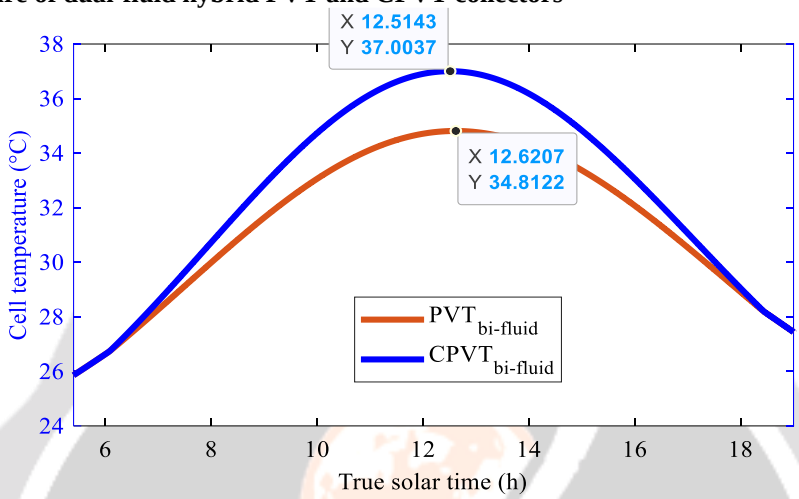

Figure 9: Cell temperature fluctuations in dual-fluid PVT and CPVT systems

Figure 9 shows the daily evolution of cell temperature in a hybrid dual-fluid PVT system, with and without solar concentration (C = 2). It can be observed that the temperature follows the solar irradiation profile, reaching a maximum of 37 °C with concentration, compared to 35 °C without concentration. This slight temperature increase highlights the effectiveness of the combined cooling system (air-water) assisted by fins, which limits cell overheating. Thus, the thermal stability ensured by this system helps maintain optimal electrical efficiency throughout the day.

3.9 Evolution of electrical characteristics (I-V and P) of dual-fluid PVT and CPVT systems

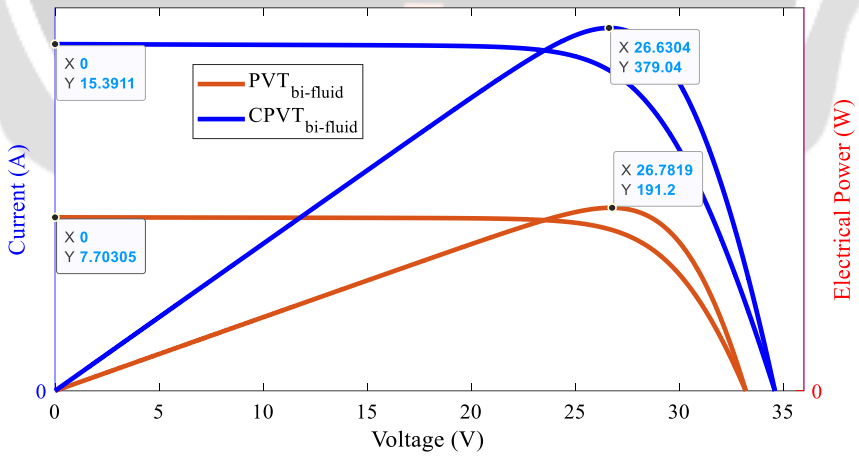

Figure 10: Comparison of I-V-P characteristics of dual-fluid PVT and CPVT modules

Figure 10 compares the I-V-P characteristics of PVT and CPVT solar collectors in dual-fluid mode (water and air used simultaneously), fitted with fins (N = 22), with air and water flow rates set at 0.028 kg.s^{-1} and 0.004 kg.s^{-1}per tube respectively. The dual-fluid CPVT collector generates a short-circuit current (Isc) of 15.39 A, approximately double that of the PVT dual-fluid (7.70 A), thanks to the concentration of solar radiation, which increases current density. Open-circuit voltages (Voc) are similar for both systems, at around 26.7 V, indicating good thermal control thanks to bi-fluid cooling and the presence of fins. In terms of maximum power, the dual-fluid CPVT reaches 379.04 W against 191.2 W for the dual-fluid PVT, reflecting a significant improvement and confirming the superiority of the

dual-fluid CPVT system for solar energy conversion. In addition, the curves show a more stable electrical behavior and a reduction in internal losses in the dual-fluid CPVT, demonstrating that the integration of a solar concentrator combined with dual-fluid cooling is a particularly effective strategy for optimizing the electrical performance of photovoltaic modules

3.10 Energy performance of dual-fluid PVT and dual-fluid CPVT systems

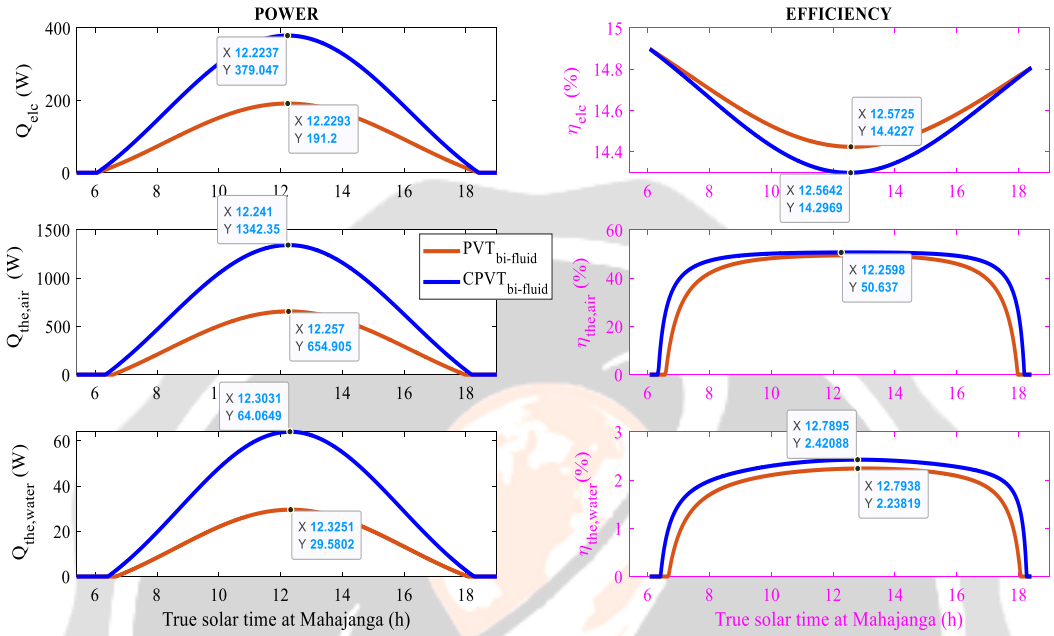

Figure 11: Evolution of the energy performance of dual-fluid PVT and dual-fluid CPVT systems

Figure 11 shows the evolution of the electrical and thermal outputs of the dual-fluid PVT and dual-fluid CPVT systems as a function of true solar time in Mahajanga. Performance follows the intensity of solar irradiation, peaking at around 12 noon, then gradually decreasing at the end of the day.

The results show that the dual-fluid CPVT system offers superior performance, both electrically and thermally, compared with the dual-fluid PVT. At its peak, the electrical power of the dual-fluid CPVT reaches 379 W, almost double that of the dual-fluid PVT (191 W). This improvement is mainly due to the integration of a solar concentrator, which increases the energy flow incident on the photovoltaic cells.

In thermal terms, power recovery is also higher for the dual-fluid CPVT : up to 1342 W for air (655 W for the dual-fluid PVT) and 64 W for water (30 W for the dual-fluid PVT). These gains are attributed to improved radiation capture and optimized heat recovery architecture.

Despite the rise in cell temperature in the middle of the day, the electrical efficiency of the dual-fluid CPVT remains stable (minimum 14.2%) thanks to a high-performance bi-fluid cooling system, compared with 14.4% for the dual-fluid PVT. This thermal control limits the degradation of photovoltaic performance.

Thermal efficiency is also in favor of the dual-fluid CPVT. The air fluid achieves an almost constant efficiency of 50% between 9 a.m. and 4 p.m., while that of water remains low (2.4%), probably due to the overall cooling of the collector induced by the high air flow rate and the integration of fins on the upper absorber plate, which reduce the internal temperature available for heat exchange with water.

4. CONCLUSION

This study has demonstrated the high potential of the hybrid dual-fluid CPVT collector for the efficient conversion of solar energy into electricity and heat. By coupling a dual-fluid photovoltaic-thermal collector (using both water and air) with a compound parabolic cylindrical concentrator, the system achieves significantly higher energy performance compared to a conventional dual-fluid PVT system.

The integration of an additional solar concentrator and a finned heat exchanger significantly enhances thermal recovery, while also allowing for a reduction in photovoltaic cell temperature through active cooling.
To theoretically determine solar irradiation, the Page model was used. The nonlinear equations governing the system were implemented in MATLAB code and solved using the Runge-Kutta method.
Numerical simulation results show that the integrated cooling system allows for a significant reduction in PV cell temperature, thereby improving their efficiency. More specifically, with a concentration factor of C = 1, the cell temperature decreases by 34.8 °C, offering an electrical efficiency of 14.4%, whereas without cooling, the temperature reaches around 65 °C in Mahajanga, according to Pasera et al. (2024) [10]. For C = 2, the temperature of the CPVT dual-fluid system's cells is reduced by 37 °C, resulting in an efficiency of 14.3%.
In terms of energy performance, the optimized electrical power of the dual-fluid CPVT reaches 379 W, compared to 191 W for the dual-fluid PVT. The maximum recovered powers for the air and water fluids reach 1342 W and 64 W, respectively, compared to 655 W and 30 W for the dual-fluid PVT system.
These results confirm the excellent potential of this hybrid system, which stands out for its ability to simultaneously maximize both electrical and thermal efficiencies. However, the performance of the dual-fluid CPVT system strongly depends on several internal parameters (heat exchanger geometry, number of fins, mass flow rate) and external parameters (solar concentration factor, ambient temperature, wind speed). Excessive use of heat-dissipating elements or poor thermal management can degrade electrical performance despite thermal gains. Therefore, optimizing operating conditions is essential to ensure a good balance between electrical production and thermal recovery.
Looking ahead, further work will aim to refine the analysis of the thermal efficiency of the dual-fluid CPVT system, particularly by studying the detailed influence of each key parameter. Thanks to its advanced design and enhanced performance, this hybrid system emerges as a credible and effective alternative for clean solar energy production, addressing the growing need for sustainable and versatile energy solutions.

5. RÉFÉRENCES

[1]. Chaker Ibrahim Omar, 'Modélisation, optimisation et gestion d'énergie d'une centrale hybride à énergie renouvelable', Thesis, University of Caen Normandie, 2023.
[2]. DONA Victorien Bruno, 'Modelisation et conversion des irradiations solaires en vue de la production d'énergie rénouvelable à Mahajanga', Habilitation to direct research, University of Mahajanga, Madagascar, August 28, 2019.
[3]. Olivier FARGES, 'Optimal design of concentrating solar power plants: application to tower power plants and 'beam down' installations. Thesis, University of Toulouse, 2014.
[4]. Tripathi, Rohit, G.N. Tiwari, 2017. 'Annual performance evaluation (energy and exergy) of fully covered concentrated photovoltaic thermal (PVT) water collector: an experimental validation'. Sol. Energy 146, 180-190.
[5]. Deepali Atheaya, A. Tiwari, G.N. Tiwari, 2016. 'Experimental validation of a fully covered photovoltaic thermal compound parabolic concentrator system'. Engineering Science and Technology an International Journal - July 2016.
[6]. Ahed Hameed Jaaz, Husam A. H., Kamaruzzaman S.,Abdul Amir H. K., Tayser Sumer G. and Ahmed A. AlAmiery , 'Outdoor Performance Analysis of a Photovoltaic Thermal (PVT) Collector with jet Impingement and Compound Parabolic Concentrator (CPC)', Materials 2017, 10, 888.
[7]. MEKADEM Hafsa and Mellouki H., 'Etude paramétrique d'un capteur hybride doté d'un concentateur parabolique composé (PVT-CPC)', Dissertation, Ahmed Draia-Adrar University, 2022.
[8]. Wenzhi Cui, Long Zhao, Wei Wu, 2010. Energy Efficiency of a Quasi CPC Concentrating Solar PV/T System', IMECE2010
[9]. TABET Ismail. 'Etude, Réalisation et simulation d'un capteur solaire', thesis, Université des freres mentouri constantine, 2016.
[10]. PASERA Joanès Keneddy, HARITHI BEN and DONA Victorien Bruno, "Optimizing the energy performance ofa hybrid PVT air collector with Parabolic trough concentrator and Heliostat", IJARIIE-ISSN(O)-2395-4396, Vol-10 Issue-5 2024
[11]. PASERA Joanès Keneddy, HARITHI BEN and DONA Victorien Bruno, 'Thermal efficiency of the Photovoltaic-Thermal air- coupled Parabolic through-Heliostat Concentrator (PVT-CCPH)', IJARIIE-ISSN(O)-2395-4396, Vol-10 Issue-6 2024.

[12]. El-YAHYAOUI Sara, 'Photovoltaıque à concentration : optimisation de l'étage secondaire', Thèse en cotutelle, Université Sidi Mohamed Ben Abdellah & Université de Lorraine, March 26, 2021.
[13]. TOUAFEK Khaled, 'Contribution à l'étude et à la conception d'un système énergétique utilisant des capteurs hybrides photovoltaïques thermiques', Thesis, Ecole Normale Polytechnique ENP, Algeria, 2010.
[14]. S. Ben Mabrouk, 'Etude et Simulation d'un Capteur hybride Photovoltaique Thermique à air', University of Tunis El Manar, Researchgate, 2016.
[15]. Oussama El Manssouri, Chaimae E. F, Bekky H et al, 'Mass Flow Rates Effect on the Performance of PV/T Bifluid Hybrid Collector (Single and Simultaneous Modes)',2021, in Electrical Engineering 681
[16]. Khelifa Abdelkrim, 'Contribution à la conception et modélisation d'un capteur solaire hybride photovoltaïque thermique PVT', Thesis, Univertsité Hadj Lakhdar de Batna, 2017.
[17]. Incropera, F.P.; DeWitt, D.P. 'Fundamentals of Heat and Mass Transfer', 6th ed; John Wiley & Sons, Inc: Hoboken, NJ, USA, 2007
[18]. GHELLAB Amel, 'Modélisation et optimisation des capteurs solaires hybrides', Thesis, Université des frères Mentours Constantine, 2018
[19]. AKERMI Mustapha, 'Modelisation, simulation et analyse de comportement d'un capteur solaire plan à eau pour différents sites en ALGERIE', These, Université Abou-bekr belkaid-Tlemcen, 2019.
[20]. GUENDOUZI Seyf eddine and LOUNIS Ibrahim, 'Performances d'un Capteur Hybride PVT/Bifluide', Memoire, Université de JIJEL, 2014.
[21]. Bourouaiah Yassine, Kimouche Fouaz, 'Etude numérique des performances d'un capteur solaire plan à eau', Memoire, Université Mohamed Seddik Ben Yahia - Jijel, 2021
[22]. BOUHOREIRA Y. and GANA L. 'Etude de l'effet des paramètres sur les performances d'un collecteur solaire cylindro parabolique', dissertation, Université Kasdi Merbah Ouargla, 24-06-2018.
[23]. René RAUD, Chapidtre I DOSSIER DE CALCULS-soleil-vapeur, March 2012.
[24]. Oussama El Manssouri, B. Hajji, Giuseppe M.T, Antonio G. and Stefano A., 'Electrical and Thermal Performances of Bi-Fluid PV/Thermal Collectors'. Energies 2021, 14, 1633.
[25]. M.Y. Othman, S.A. Hamid et al, Performance analysis of PV/T Combi with water and air heating system: An experimental study. Renewable Energy 86 (2016) 716e722
[26]. Nurul Shahirah Rukman, Ahmad F. et al, Bi-fluid cooling effect on electrical characteristics of flexible photovoltaic panel, Journal of Mechatronics, Electrical Power, and Vehicular Technology 12 (2021) 51 -56
[27]. Mohammad Sardarabadi, Mohammad P., Experimental and numerical study of metal-oxides/water nanofluids as coolant in photovoltaic thermal systems (PVT), Solar Energy Materials & Solar Cells 157 (2016) 533-542
[28]. Hasila Jarimi, Mohd Nazari A. B., et al, Bi-fluid photovoltaic/thermal (PV/T) solar collector: experimental validation of a 2-D theoretical model, Renewable Energy 85 (2016) 1052 e1067
[29]. F.Sarhaddi, S. Farahat, et al, An improved thermal and electrical model for a solar photovoltaic thermal (PV/T) air collector, Applied Energy 87 (2010) 2328-2339
[30]. BELKACEM Mourad, 'Etude et optimisation du transfert d'énergie électrique en conversion photovoltaïque par la recherche du point de puissance maximal (MPPT)', Dissertation, Université Abou Belkaid de Tlemcen, 2015.